Schlieren-based temperature measurement inside the cylinder of an optical spark ignition and homogeneous charge compression ignition engine

Pavlos Aleiferis[1,3], Alexandros Charalambides[1,4], Yannis Hardalupas[1], Nikolaos Soulopoulos[1], A.M.K.P. Taylor[1,*] and Yunichi Urata[2]

[1]Department of Mechanical Engineering, Imperial College London, Exhibition Road, London SW7 2BX, UK
[2]Honda R & D Co., Ltd., Tochigi R&D Centre, Tochigi 321-3393, Japan
[3]Present Address: Department of Mechanical Engineering, University College London, London, WC1E 7JE, UK
[4]Present Address: Department of Environmental Management, Cyprus University of Technology
*Corresponding author: a.m.taylor@imperial.ac.uk

Schlieren [1, 2] is a non-intrusive technique that can be used to detect density variations in a medium, and thus, under constant pressure and mixture concentration conditions, measure whole field temperature distributions. The objective of the current work was to design a schlieren system to measure line-of-sight averaged temperature distribution with the final aim to determine the temperature distribution inside the cylinder of Internal Combustion engines. In a preliminary step, we assess theoretically the errors arising from the data reduction used to determine temperature from a schlieren measurement and find that the total error, random and systematic, is less than 3%, for typical conditions encountered in the present experiments. A Z-type, curved-mirror schlieren system was used to measure the temperature distribution from a hot air jet in an open air environment in order to evaluate the method. Using the Abel transform, the radial distribution of the temperature was reconstructed from the line of sight measurements. There was good agreement in the peak temperature between the reconstructed schlieren and thermocouple measurements. Experiments were then conducted in a four-stroke, single-cylinder, optical spark ignition engine with a four-valve, pentroof-type cylinder head to measure the temperature distribution of the reaction zone of an *iso*-octane-air mixture. The engine optical windows were designed to produce parallel rays and allow accurate application of the technique. The feasibility of the method to measure temperature distributions in IC engines was evaluated with simulations of the deflection angle combined with equilibrium chemistry calculations that estimated the temperature of the reaction zone at the position of maximum ray deflection as recorded in a schlieren image. Further simulations showed that the effects of exhaust gas recirculation and air-to-fuel ratio on the schlieren images were minimal under engine conditions compared to the temperature effect. At 20 crank angle degrees before top dead centre (i.e. 20 crank angle degrees after ignition timing), the measured temperature of the flame front was in agreement with the simulations (730–1320 K

depending on the shape of the flame front). Furthermore, the schlieren images identified the presence of hot gases ahead of the reaction zone due to diffusion and showed that there were no hot spots in the unburned mixture.

OCIS codes: (1740) Combustion diagnostics; (2740) Geometric optical design; (100.0100) Image processing; (110.0110) Imaging systems; (2960) Image analysis; (6780) Temperature;

http://dx.doi/org/10.1364/AO.99.099999

1. Introduction

The aim of the present work is to develop a schlieren technique to measure the temperature distribution inside the cylinder of an optical internal combustion (IC) engine, running in either Spark Ignition (SI) or Homogeneous Charge Compression Ignition (HCCI) mode. The schlieren technique has been largely used as a visualization tool to study combustion in IC engines, but it can also be used for in-cylinder temperature measurements. Since the technique relies on the deflection of light caused by naturally-occurring density gradients, without the need for additives or tracers, it holds an advantage in measuring the temperature distribution and stratification in an HCCI engine prior to autoignition, given the sensitive autoignition chemistry.

The schlieren technique has been broadly applied to flow visualisation – e.g., for capturing shock waves and locating flame fronts – but, also, in quantitative measurements of temperature or concentration in isothermal and reacting flows [3-6]. The high sensitivity of the technique to gas temperature and concentration inhomogeneities along the light path allows its wide applicability, but, at the same time, becomes problematic in certain situations, for example, when curved windows enclose the test area; in fact, a majority of the reported quantitative schlieren measurements have been performed in open environments or using flat windows. In particular, curved windows will act as lenses and deflect the parallel light beam used in schlieren experiments, which will render the schlieren images hard to interpret. Consequently, the application of the technique in interesting environments, such as the in-cylinder flow field of an IC engine, requires special attention. Previous attempts at using qualitative schlieren visualisation in situations where optical access is provided through curved optical surfaces in engines have been reported in [7-9]. One approach places appropriate lenses in front and after the curved engine cylinder windows [8], aiming to reshape the incoming parallel light when it passes through the engine cylinder. The lenses can be specially designed, including a detailed assessment of their aberrations, so provide flexibility in the experimental setup [9]. Alternatively, the whole engine cylinder can be manufactured in such a way as to keep the incoming light collimated through the engine [7]. In our experiments, optical access to the IC engine is provided through pentroof windows, which we specially design to maintain parallel light through the engine and, also, avoid

possible complications due to relative movement between the engine and a fixed lens. Additionally, in contrast to previous efforts, we aim to make (semi-) quantitative measurements using the improved optical access.

Extracting quantitative temperature information from a schlieren image requires the appreciation of the line-of-sight (LOS) averaged nature of the resulting measurement and, also, an assessment of the experimental errors caused by the combined effects of temperature and concentration on the light deflection.

The two-dimensional projection of the three-dimensional in-cylinder temperature field of an HCCI engine is particularly useful. The random nature of auto-ignition sites in the entire volume of these engines precludes the use of 2D planar measurements and the relatively large cylinder volume during auto-ignition is not currently accessible using 3D laser diagnostics, exacerbated by the restricted optical access in the cylinder pentroof. However, the schlieren-derived average temperature is not a simple average of the temperature along a line-of-sight, but a complex weighted average of the temperature distribution. So, it is more common to measure the temperature of reacting gases in axisymmetric configurations, combined with the use of tomographic reconstruction. Despite the difficulty in interpreting the non-axisymmetric temperature projections, it is possible to produce bounds for the resulting bias between an intuitive arithmetic average temperature and the line-of-sight-averaged temperature, which results from a schlieren measurement.

A potential impediment in the application of schlieren inside the cylinder of an IC engine is the existence of unknown variations in both the temperature and the gas composition and their combined effect on the refractive index. For methane-air, partially premixed, atmospheric combustion, [10, 11] used laminar flame calculations to show that an error in temperature of less than 10% can occur when not accounting for composition variations, depending on the equivalence ratio. However, inside the cylinder of an IC engine there are differences. The fuel used is generally a heavier hydrocarbon, which has a larger refractive index than air, and the pressure and temperature are elevated with respect to the atmospheric values; furthermore, the potential existence of Exhaust Gas Recirculation (EGR) creates more uncertainties on the effect of composition on the refractive index.

Quantitative schlieren measurements have been long attempted, using either a Z-type system [12] or rainbow schlieren [13], measuring the refractive index and the density fields. Temperature measurements were attempted in isothermal flows [6, 14] using rainbow schlieren and it was shown that the temperature rise could be accurately evaluated. Measurements of temperature in flames followed, typically in laminar premixed flames, where composition variations in rich jet flames [4] or spherical microgravity flames [15] affected the measured temperature to within a few percent and the derived temperature agreed very well with thermocouple measurements; however, for heavier hydrocarbon fuels extra effort is required to model composition effects [16].

Temperature measurements using Z-type schlieren systems were demonstrated in turbulent flames employing multiple-angle tomography [5], rather than the Abel transform used in the previous studies, and in semi-2D convective layers [17], also demonstrating good accuracy. Most of existing quantitative studies used experiments with ample optical access and basic flow configurations; however, in many important cases, like inside the cylinder of IC engines, optical access can be restricted and the flow field is not symmetric. In these cases, even the LOS-averaged refractive index or temperature distributions prove beneficial, provided that reasonable bounds on the variation of these quantities can be calculated.

The next section presents the theory of the schlieren technique. Section 3 presents an analysis of the errors in schlieren-based temperature measurements, which are caused by the line-of-sight averaged nature of the refractive index measurement and the subsequent determination of temperature through the density. Sections 4 and 5 show an experimental evaluation of temperature measurements using schlieren in a controlled environment, while making use of Abel transform to reconstruct line-of-sight measurements. Section 6 presents the experimental arrangement in a SI engine, the design of the optical windows to allow schlieren measurements and possible sources of error and section 7 presents in-cylinder temperature measurements from the engine experiments. The paper ends with a summary of the main findings.

2. Schlieren technique

Light propagates uniformly through a homogeneous medium. However, where there are inhomogeneities in the medium (e.g. a variable temperature field), the density of the medium changes and therefore its refractive index also changes. A beam of parallel light will therefore be deflected when passing through this medium. For gases, there is a simple relationship between density and refractive index:

$$n - 1 = k\rho \qquad \text{Equation 1}$$

where n is the refractive index, ρ is the density and k is the Gladstone-Dale coefficient, generally called "refractivity", which is a gas property with a value, for air, of about 0.23 cm^3/g. Here, the objective was to use the schlieren method to measure this change in density. We first consider a lens-based schlieren system, shown in Fig. 1.

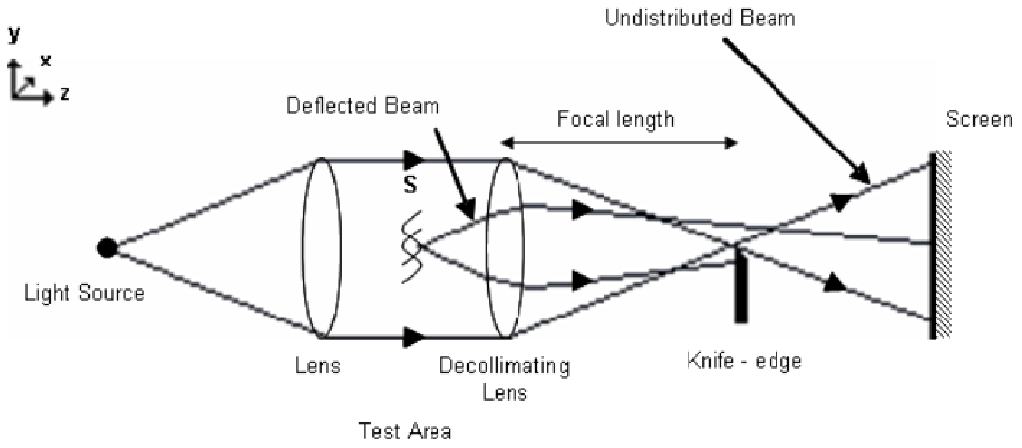

Fig. 1. Diagram of a Lens-based schlieren System. Reproduced from [2].

In Fig. 1, x, y, z is the co-ordinate system, where we take the z-axis in the parallel direction to the line of sight and the origin of the system being equidistant between the two lenses, at the centre of inhomogeneity S(x,y,z); S(x,y,z) denotes the inhomogeneity in the medium due to temperature variation. A knife-edge with the longest dimension parallel to the x-direction is used to block off the rays of light that have not deviated from their "undisturbed", - parallel to the axis of the lens - direction (*i.e.* in the x,y-plane). In this way, only the rays that were deflected due to inhomogeneity S(x,y,z) in the positive y-direction will illuminate the screen. The first spherical lens is used to collimate rays from the light source, while the second is used to focus the rays in the plane of the knife-edge. As it will be explained later in this section, by studying the intensity distribution on the screen, we can calculate the angular deflection of the rays and therefore the change in the refractive index using the equation [2]:

$$\varepsilon_y = \frac{1}{n_0}\int \frac{\partial n}{\partial y} dz \qquad \text{Equation 2}$$

where ε_y is the angular deflection of the ray in the y-direction, n_0 is the refractive index of the surrounding medium and $\partial n/\partial y$ is the rate of change of the refractive index in the y-axis direction.

As shown in Equation 1, the density of the inhomogeneity can be found from the refractive index of the medium and the temperature of the inhomogeneity can also be found by using the perfect-gas state equation,

$$\frac{p}{\rho} = RT \qquad \text{Equation 3}$$

where p is the absolute pressure, T is the temperature of the inhomogeneity and R is the specific gas constant.

Briefly in [18] and in more detail in [19], an analysis was presented as to how to calculate the temperature field from the intensity variations of an image projected on the screen. For a known focal length decollimating lens,

$$\Delta\alpha = f\varepsilon_y \qquad \text{Equation } 4$$

where $\Delta\alpha$ is the deflection of the beam away from the knife edge in the y-direction and f is the focal length of the decollimating lens, as indicated in Fig. 1. The deflection angle, ε_y, of the light beam passing through an inhomogeneity can be calculated using the equation:

$$\frac{I_d - I}{I} = \frac{\Delta\alpha}{\alpha_k} \approx \pm\frac{f}{\alpha_k}\varepsilon_y \qquad \text{Equation } 5$$

where I_d is the illumination of the image of the disturbed field, I is the illumination of the image of the undisturbed field and α_k is the dimension of the undisturbed image above the knife edge in the y-direction. The ± sign depends on the position of the knife edge (i.e. indicating whether the knife edge cuts off the rays in the negative or positive y-direction, respectively). The variables used in Equation 4 and Equation 5 are illustrated in Fig. 2.

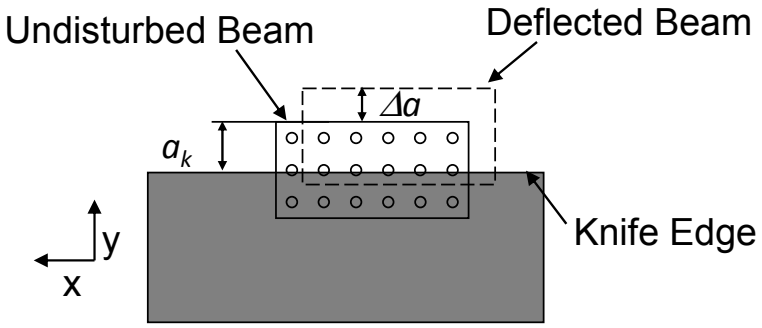

Fig. 2. Position of disturbed and undisturbed beam at the knife edge. Reproduced from [19].

Equation 2 and Equation 5 can be further analysed to calculate the change in the refractive index along the ray path from the deflection angle [20, 21]:

$$\frac{I_d - I}{I} = \pm\frac{f}{\alpha_k}\varepsilon_y = \pm\frac{f}{\alpha_k n_0}\int\frac{\partial n}{\partial y}dz \qquad \text{Equation } 6$$

Using Equation 3 and the Gladstone-Dale relation, Equation 1, we can calculate the LOS-averaged temperature variation along the ray path by rearranging:

$$\frac{I_d - I}{I} = \pm\frac{f}{\alpha_k n_0}\int\left(\frac{n_0 - 1}{\rho_0}\right)\frac{p}{RT^2}\frac{\partial T}{\partial y}dz \qquad \text{Equation } 7$$

to

$$\frac{\partial\langle T\rangle}{\partial y}\frac{1}{\langle T\rangle^2}=\pm\frac{I_d-I}{I}\frac{\alpha_k n_0}{fL(x)}\frac{\rho_0}{n_0-1}\frac{R}{p} \qquad \text{Equation 8}$$

where <*T*> is the LOS-averaged temperature along *L(x)*, n_0 and ρ_0 are a reference refractive index and a reference density, respectively, so that $k=(n_0-1)/\rho_0$ and *R* and *k* depend on gas composition. In arriving at Equation 8, we approximated the LOS-averaged temperature as

$$\int\frac{1}{T^2}\frac{\partial T}{\partial y}dz=\frac{1}{\langle T\rangle^2}\frac{\partial\langle T\rangle}{\partial y}L(x) \qquad \text{Equation 9}$$

The LOS-averaged temperature is calculated by numerically integrating Equation 8, whose right hand side is the measurement of light deflection. We used an Euler scheme for the integration along the y-direction starting at y0=0; at this location a "datum" line of known temperatures along the x-direction is required for the calculation of the LOS temperature distribution. The length *L(x)* depends on the size of the inhomogeneity along the light path and in the engine measurements the width of the combustion chamber was used at every y-location.

In the experiment to be described in section 0, a schlieren system with a horizontal knife edge (instead of a radial filter or a vertical knife edge) was used due to the shape of the optical windows inserted on the cylinder wall of the pentroof of the internal combustion engine. The pentroof windows deflect the light beam from the collimator lens in the x-direction, prohibiting the use of a radial filter or a vertical knife edge. However there is no deflection in the y-direction from the pentroof windows and therefore a horizontal knife edge can be used.

3. Errors in LOS-averaged temperature measurement

The calculation of the LOS-averaged temperature from a schlieren measurement includes both systematic and random errors. The systematic errors are due to the non-linear dependence of temperature on refractive index (and density) and the random errors are due to experimental noise.

The bias introduced through the LOS-averaged temperature approximation we use, Equation 9, as compared to an arithmetic temperature average is explained as follows: We can write Equation 6 as$\langle\partial\rho/\partial y\rangle=\partial\langle\rho\rangle/\partial y=(a_k n_0\rho_0/f(n_0-1))\cdot((I_d-I)/I)/L(x)$ (square brackets, ⟨ ⟩, denote a LOS-averaged quantity). There are, then, two possible ways to proceed in order to calculate the LOS-averaged temperature. At first, the integration of the previous equation gives the LOS-averaged density, $\langle\rho\rangle$ and we have$\langle\rho\rangle=(p/R)\langle 1/T\rangle$, however$\langle 1/T\rangle\neq 1/\langle T\rangle$. Alternatively, the method described in the previous section uses$\langle\partial\rho/\partial y\rangle=(-p/R)\langle 1/T^2\cdot\partial T/\partial y\rangle$, however$\langle 1/T^2\cdot\partial T/\partial y\rangle\neq 1/\langle T\rangle^2\cdot\partial\langle T\rangle/\partial y$. So, in either case, the non-linear dependence of temperature on refractive index demands certain approximations to infer the LOS-averaged temperature from the measurement.

The various errors in the calculation of the LOS-averaged temperature arise from: (i) the bias introduced through the average used in Equation 9 as explained above, (ii) the integration procedure used to calculate the temperature from the measurement of its derivative, (iii) the uncertainty in the datum temperature value, (iv) the noise fluctuations in the measurement (the random error associated with the measurement of I_d in Equation 8) and (v) the effect of the local turbulent fluctuations as they accumulate in the measurement (since a given turbulent distribution of temperature will give different LOS-averaged temperatures, depending on the average definition used).

In order to assess these errors, we construct two-dimensional slices (*i.e.* planes parallel to the light direction) of 3D temperature fields, where the optical setup is as in Fig. 1, using the following equation

$$T(y,z) = \frac{\partial T(y,z)}{\partial y} \cdot \Delta y + T_d \qquad \text{Equation 10}$$

where T_d is the "datum" temperature. In every field, the horizontal (along z) variation of the temperature and the normal temperature derivative (∂T/∂y) follow error functions and the vertical (along y) variation of temperature is linear – at the lowest y the temperature is constant and the vertical gradient changes for different values of z. The values of temperature and the domain dimensions are chosen so as to be relevant to the engine measurements that will be described later and the magnitude of the maximum vertical variation of the temperature, *i.e.* the maximum ∂T/∂*y* is called temperature stratification.

Using the above temperature fields, we calculate the arithmetic temperature average $\langle T(y)\rangle_{ar} = (1/L)\int_0^L T(y,z)dz$ and the LOS-averaged temperature as described in the previous section, $\langle T(y)\rangle_{sch}$. The quantity $e = 1 - \langle T\rangle_{sch}/\langle T\rangle_{ar}$ quantifies the bias of the schlieren-derived temperature with respect to the arithmetic average and depends on: i) the temperature difference along a LOS, ii) the minimum and maximum temperature in any given temperature field, iii) the values and the range of ∂T/∂y along a LOS and iv) the "datum" temperature.

We can anticipate the behaviour of the bias by considering an Euler scheme for the integration of Equation 9 and comparing it with a hypothetical integration for the arithmetic average of the temperature. Equation 9 can be integrated as (T_1 and T_2 correspond to temperatures at adjacent y-locations) $\langle T_2\rangle = \langle T_1\rangle + dy \cdot \langle T\rangle^2 \cdot f_s(T,y)$, where, $f_s(T,y) = (1/L)\int_0^L 1/T^2 \cdot \partial T/\partial y \cdot dz$ and the arithmetic average can be integrated as $\langle T_2\rangle = \langle T_1\rangle + dy \cdot f_a(T,y)$, where $f_a(T,y) = (1/L)\int_0^L \partial T/\partial y \cdot dz$. Then, the difference between the arithmetic and the schlieren LOS-averaged temperatures is attributed to the behaviour of the ratio $(\langle T\rangle/T)^2$. To the extent this ratio diverges from 1, the calculated temperature becomes more and more different from the arithmetic average. As an

example, Fig. 3 shows how the vertical temperature derivative changes due to the ratio$(\langle T\rangle/T)^2$; the consequence of this 'modulation' of the vertical temperature derivative is a lower schlieren LOS-averaged temperature.

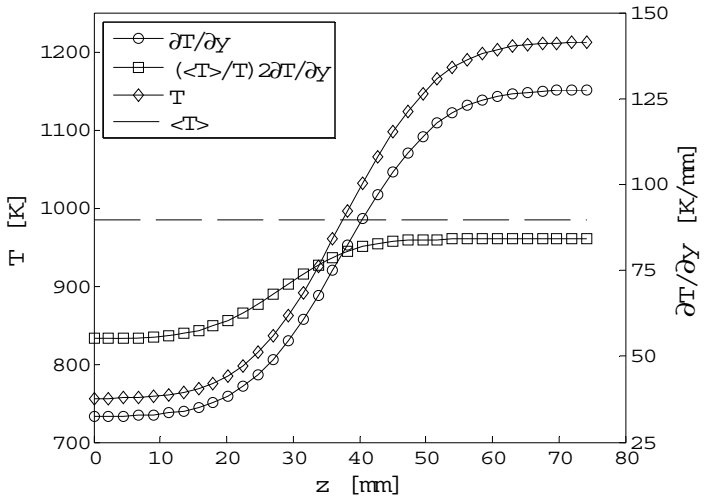

Fig. 3. The variation, along the LOS direction, of the vertical temperature derivative and the 'modulated' vertical temperature derivative due to the term$(\langle T\rangle/T)$. Also shown is the temperature profile along the LOS.

Fig. 4 shows the quantity *e*, plotted as a function of the temperature increase along the line-of-sight, ΔT_{LOS}, and of the maximum temperature difference in the field, ΔT. The worst bias is about 8%, but for typical conditions it stays below 5%. It follows from the explanation above that starting from a given "datum" temperature, the bias increases as the temperature range of the measurements increases; this temperature range can be manifested either as the temperature difference along a LOS or as the overall temperature range in the field. Furthermore, for the same vertical temperature gradient, the bias decreases with increasing "datum" temperature (*c.f.* curves 'o' and '◊' in Fig. 4). To explain this, consider two temperature distributions with the same range of temperatures, *i.e.* ΔT, but different actual temperature values. The same temperature range is a smaller percentage of the larger average temperature than of the lower one, so the ratio $\langle T\rangle/T$ is smaller in the former case.

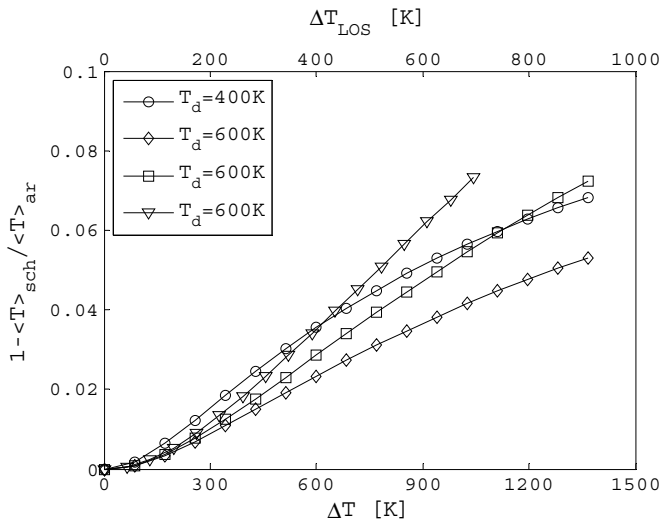

Fig. 4. The error quantity$e = 1 - \langle T \rangle_{\mathrm{sch}} / \langle T \rangle_{\mathrm{ar}}$, where $\langle T \rangle_{\mathrm{sch}}$ is the schlieren LOS-averaged temperature and $\langle T \rangle_{\mathrm{ar}}$is the arithmetic average, as a function of the temperature difference along a LOS and overall temperature difference in the field. T_d is the "datum" temperature, *i.e.* the known temperature used to start the integration. The maximum temperature gradients are '○' 150 K/mm; '◊' 150 K/mm; '□' 128 K/mm; '▽' 83 K/mm.

In addition, when the actual values of the temperature gradient decrease, the bias slightly increases, when keeping the "datum" temperature the same (*c.f.* curves '◊' and '□' in Fig. 4, which have the same range of vertical temperature gradients). Decreasing the "datum" temperature, also, tends to increase the bias (*c.f.* curves '○' and '□' in Fig. 4). Finally, as both the range and the actual values of the vertical temperature gradient decrease, the bias starts to become larger (*c.f.* curve '▽' in Fig. 4).

The value of the "datum" temperature needs to be known in order to calculate the LOS-averaged temperature from the schlieren measurement. The error introduced by the uncertainty in the value of the "datum" temperature is shown in Fig. 5. The error quantity $e = 1 - \langle T \rangle_{\mathrm{sch}} / \langle T \rangle_{\mathrm{ar}}$, as in , where the error is calculated for the correct datum temperature and for values around the correct one. The effect of this uncertainty is to add a maximum of 3% to the bias of the schlieren LOS-averaged temperature.

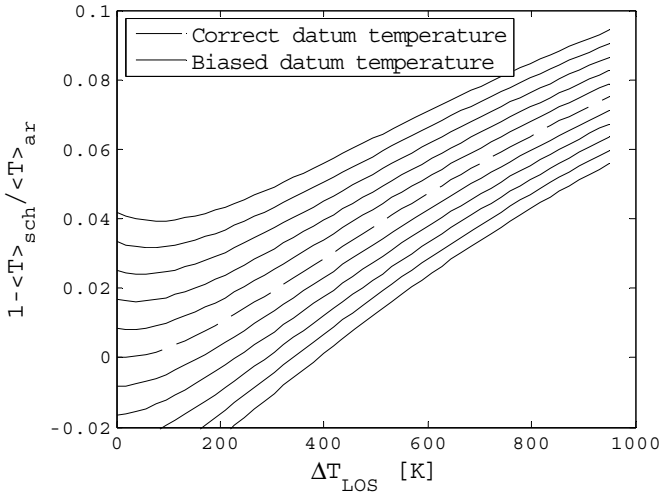

Fig. 5. The error quantity $e = 1 - \langle T \rangle_{\mathrm{sch}} / \langle T \rangle_{\mathrm{ar}}$, as in Fig. 4, for different "datum" temperatures. The dashed line is the correct "datum" temperature and the solid lines are ±25K around the correct value. The maximum difference is about 3%.

The effect of random measurement errors is assessed by assuming that the measured quantity, Equation 8, follows a Gaussian probability distribution, with the mean equal to the value calculated in the above analysis and the standard deviation equal to 2% of the maximum value, for every LOS. This value corresponds to the standard deviation of the actual measurement using the hot-air gun experiment – which is described in ~~the following~~ section 4 – at locations of constant temperature, *c.f.* the leftmost part of the profile in Fig. 12; the Gaussian distribution is a good approximation for the measured values at this portion of the profile. Fig. 6 shows the result, where 100 different realisations of the measurement are used to produce as many temperature bias distributions. As an estimate of the random error, we use the standard deviation around the mean bias, which gives a maximum value for the random error in the temperature bias of ~0.2% (assuming a 5% standard deviation for the measurement error, instead of 2%, gives a value for the standard deviation of the bias of ~0.5%).

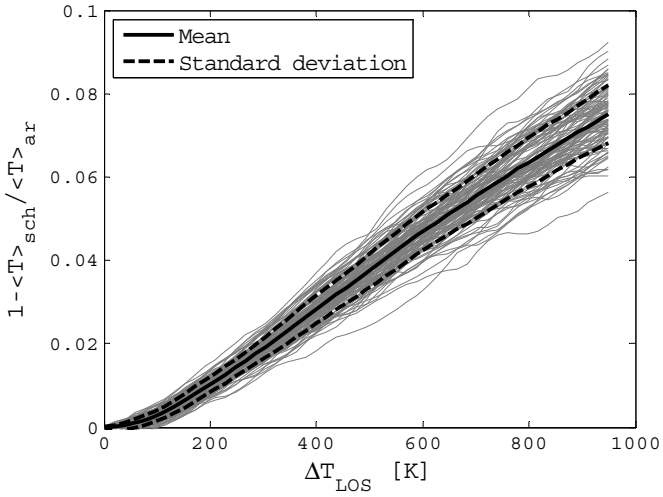

Fig. 6. The error quantity $e = 1 - \langle T \rangle_{\mathrm{sch}} / \langle T \rangle_{\mathrm{ar}}$, as in Fig. 4, showing the effect of measurement noise. The light curves are the errors for 100 different realisations of the measurement, the solid line is the average error (which is the same as in Fig. 4) and the broken lines denote one standard deviation around the mean. The maximum standard deviation of the bias is around 0.2%.

Finally, we assess the effect of turbulent temperature fluctuations on the LOS-averaged temperature, by allowing the temperature and temperature derivative profiles that were used in the initially constructed 2D temperature field to fluctuate around a mean value. The probability density function of the fluctuations is, again, considered Gaussian with mean as calculated initially and standard deviation 10% of the maximum temperature, for every LOS. Fig. 7 shows that errors in this case are very similar as in the assessment of the random measurement error above; the estimated maximum standard deviation of the bias is ~0.5%.

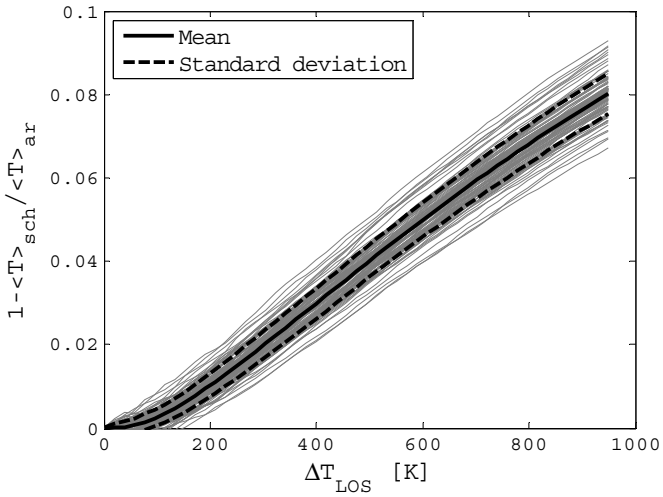

Fig. 7. The error quantity $e = 1 - \langle T \rangle_{\mathrm{sch}} / \langle T \rangle_{\mathrm{ar}}$, as in Fig. 4, showing the effect of turbulent fluctuations. The light curves are the errors for 100 different realisations of the measurement, the solid line is the average error (which is almost the same as in Fig. 4) and the broken lines denote one standard deviation around the mean. The maximum standard deviation of the bias is around 0.5%.

The above sources of error are independent of each other, so can be added in quadratic form to arrive at the total error for the LOS-averaged temperature, for the range of temperatures expected in the following engine experiments and the assumed temperature profiles shown in Fig. 3. Practically, the systematic error contribution from the definition of the LOS-averaged temperature dominates the total error. The maximum error is ~6%. However, this value corresponds to extreme cases considered and we expect the error to be typically ~3%. The analysis presented here assumes that temperature differences are the only cause of change in refractive index. This is verified in section B, which indeed shows that the temperature causes most of the light beam deflection. So, the present error estimates provide a suitable upper bound for the error in the LOS-averaged temperature from schlieren measurements, for the conditions considered in the present work.

4. Validation experiments

Inside the cylinder of an IC engine, the variation in the refractive index measured by the schlieren technique depends on both temperature and concentration changes. So, initially, the two effects were isolated in order to evaluate the ability of the schlieren setup to measure temperature. A rig was constructed to test the accuracy of the temperature measurements and assess the developed algorithm for processing schlieren images in a non-ideal, non-symmetrical turbulent flow field before attempting to measure the temperature distribution in the engine. In this environment no additional variation of concentration is present, so only temperature affects the measured refractive index. A small hot air gun was placed in the test region and when turned on, the temperature of the hot air jet caused changes in the density of the medium. A Z-type schlieren System, – its name originating from the optical arrangement forming the letter Z – was used due to space limitations in our laboratory [1]. The developed Z-type schlieren system is shown in Fig. 8, based on two parabolic mirrors of 3000mm focal length and 150 mm diameter, instead of lenses. A 75W halogen lamp and a 6×2mm slit were used to produce a uniform intensity distribution from a light source. In Fig. 8 paths 1 and 3 were at an angle of 6º from path 2.

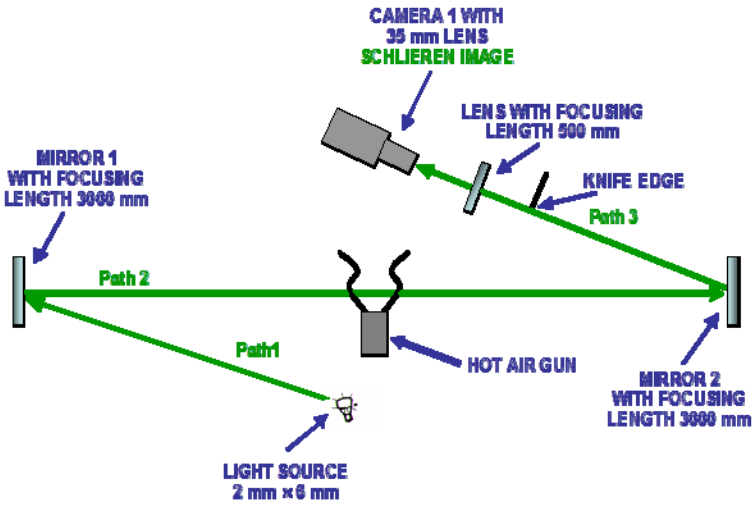

Fig. 8. Optical setup of a Z-type schlieren system.

An 8bit, 768×576pixels Charge Coupled Device (CCD) camera with Nikon UV-Nikkor 35mm, f/4.5 lens was used to capture the schlieren image. The camera had a frame rate of 25 Hz and was coupled to an image intensifier (the same setup as in the engine experiments described in section 6); the schlieren image was acquired using a long exposure time to provide an average distribution. Fig. 9 shows two images of the test region: one with the hot air gun turned off (*i.e.* undisturbed field) and one with the hot air gun turned on (*i.e.* disturbed field).

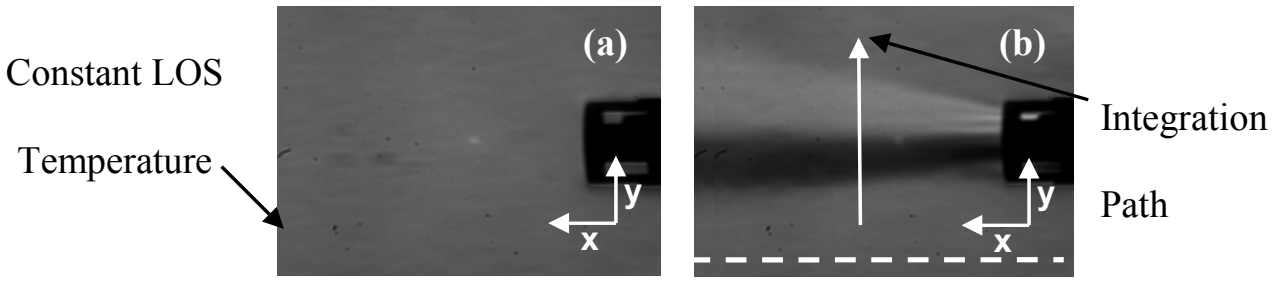

Fig. 9. Example schlieren images. (a) undisturbed field, I and (b) disturbed field I_d for the hot air jet. The jet diameter is 20 mm.

In order to evaluate the temperature distribution as measured using the schlieren technique, we selected a grid with 97 points to measure the temperature of the jet using a K-type thermocouple. The thermocouple was placed in the vertical plane of symmetry of the hot air gun and it was traversed at 10mm intervals; while at the exit of the hot air gun, the grid was denser with the thermocouple traversed in 5mm intervals as shown in Fig. 10, where the white dots represent the thermocouple measurement locations.

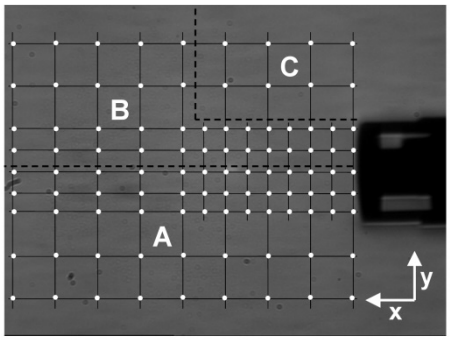

Fig. 10. Thermocouple grid used to characterise the temperature distribution in the hot air jet.

The LOS-averaged temperature distribution of the hot air gun as calculated from the schlieren images, according to the method described in Section 2, and the temperature distribution calculated by interpolating the thermocouple measurements are shown in Fig. 11. *L(x)* was varied from 20mm at the exit of the gun to 40mm downstream in the hot air jet.

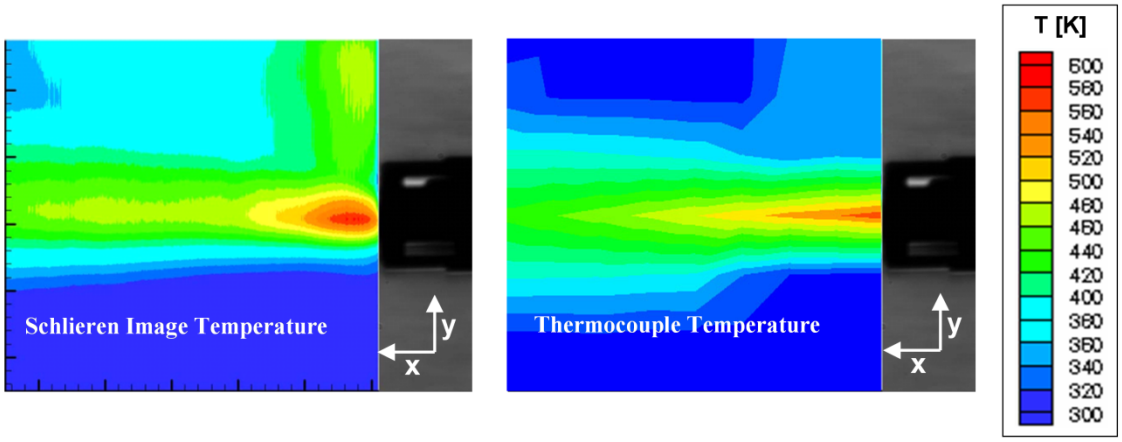

Fig. 11. Line of sight temperature distribution from the hot air jet using schlieren measurement (left) and temperature distribution from the hot air jet using point thermocouple measurements (right).

The results show that the maximum temperature of the hot air gun at the jet exit is about 600 K. The thermocouple measurement grid was divided in 3 sections (shown in Fig. 10 by the dashed lines), because the difference between the thermocouple point temperature and the one calculated from the schlieren image varied at different sections of the schlieren image. A x-y coordinate system was used with its origin being at the centre of the exit of the hot air gun, with y-values increasing as we move upwards of the centerline and x-values increasing with downstream distance. Section A included all the grid points from the centerline of the hot air gun and for

y<0mm (for all values of x). Section B included the grid points (a) within the hot air gun jet for y>0mm (0<y<20mm for 0<x<40mm and 0<y<40mm for x>40mm) and (b) within the gas area furthest away from the hot air gun mouth (y>40mm for x>40mm) whose temperature was slightly affected by the hot air gun operation. Finally, Section C included all the grid points within the area closest to the hot air gun exit (y>20mm for x<40mm), whose temperature was affected by the hot air gun operation. All three Sections are indicated in Fig. 10 with the dashed lines. The image area was separated in the above three sections due to the variations in the above-mentioned difference that varied significantly depending on the presence of the hot gases. By calculating the difference in the measured temperatures from the K-type thermocouple and the ones estimated by the schlieren method, the average error was 4% in section A, 20% in section B and 28% in section C. These differences are to be expected, since the comparison is between point thermocouple measurements and line-of-sight averaged schlieren temperature measurements. Overall, there was reasonable agreement of the temperature distribution between the thermocouple and the schlieren data.

5. Abel transform

The hot air gun experiment can also be used to evaluate the temperature measurements with the schlieren technique in a different way; *i.e.* to invert the LOS data in order to obtain point measurements of the refractive index and, subsequently, of temperature. In this way, a direct comparison with the point measurements of the thermocouple can be performed. In the context of the hot air gun experiment, where the flow could be considered axially symmetric, this is most easily accomplished by using an Abel transform. In this case, using $\delta = n/n_0 - 1$ (n_0 being the refractive index of the surroundings) and the change of variables $r^2 = z^2 + y^2$ (the origin of the coordinate system being at the axis of symmetry), Equation 2 can be written as

$$\varepsilon_y = 2y \int_y^\infty \frac{d\delta}{dr} \frac{dr}{\sqrt{r^2 - y^2}} \qquad \text{Equation 11}$$

where δ is a function of only the radius r.

The above integral, Equation 11, can be inverted to obtain the radial distribution of δ and the Abel inversion is, [22], $\delta(r) - \delta(r_{ref}) = J(r) - J(r_{ref})$, where

$$J(r) = -\frac{1}{\pi} \int_r^\infty \frac{\varepsilon_y dy}{\sqrt{y^2 - r^2}} \qquad \text{Equation 12}$$

The location r_{ref} is a reference location point, where the value of the refractive index is accurately known. The integral $J(r)$ was performed semi-analytically in [23] (following an equivalent procedure as in [24]) and was shown

to be given by $J_i = D_{ij}\varepsilon_j$, where the exact form of D_{ij} is given in [23] and summation over the indices *j* is implied. The temperature is given by $T = \frac{\delta_0 T_0}{\delta}$, [2], where subscript 0 refers to a location where the temperature and the refractive index are known with accuracy; in what follows this location is the ambient environment, where T_0 = 293K and $\delta_0 = 2.926\times10^{-4}$; note that this location might be different from the location of r_{ref} .

The accuracy of the calculated temperature using the above procedure depends on the measurement accuracy and on the reference location chosen for the calculation of the Abel inversion integral. Choosing the reference point at some hot location in the flow is a better choice than the cold ambient, [2], and a flame location was shown to produce lower uncertainties [16]. In the present, the reference point at each downstream station was chosen, from the thermocouple measurements, at the centreline of the hot air jet. The uncertainty in δ is$\Delta\delta = \Delta J + \Delta J_{ref} + \Delta\delta_{ref}$. The uncertainty in δ_{ref} is$\Delta\delta_{ref} = \frac{\delta_0 T_0}{T^2}\Delta T$, showing that larger reference temperatures produce smaller uncertainties in the refractive index. The uncertainty in the integral is $\Delta J_i = D_{ij}\Delta\varepsilon_j$, where the uncertainty in the measured deflection angle, Equation 5, is given by $|\Delta\varepsilon|/|\varepsilon| = \sqrt{(\Delta a_k/a_k)^2 + (\Delta I_d/I_d)^2}$; both uncertainties in this expression were estimated at 10%. This form of uncertainty for the integral can account for varying (as a function of radial distance) errors in the deflection measurements. This relationship also shows that for points near the jet axis the uncertainty accumulates from all points in the measurement domain, resulting in a larger error as the centreline is approached. Combining all the uncertainties accounts for the overall uncertainty in the reconstructed temperature

$$\Delta T = \frac{T^2}{\delta_0 T_0}\Delta\delta \qquad \text{Equation 13}$$

demonstrating, in turn, that locations of high temperature have larger errors than colder regions.

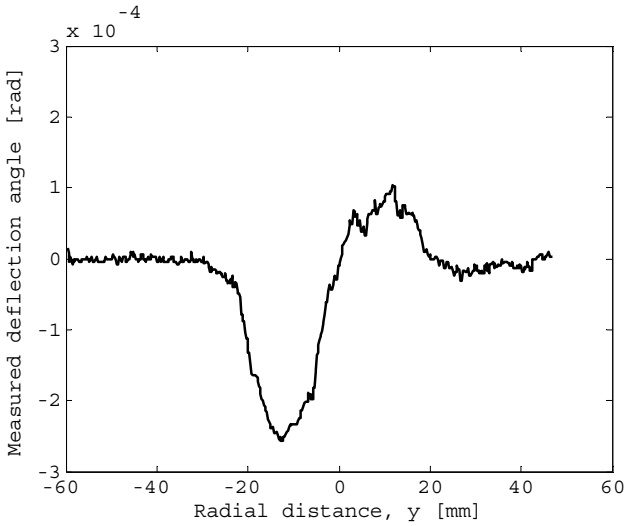

Fig. 12. The measured deflection angles, Equation 5, 20 mm downstream of the nozzle exit in the hot air jet experiment. The integration direction is from negative to positive y.

Fig. 12 shows an example of a measured deflection angle profile at 20 mm downstream of the jet exit. Fig. 13 shows, for two downstream locations, the measured temperature using the thermocouple and the calculated temperature from the schlieren images, where the error bars correspond to the uncertainties calculated with the above methodology. For axial locations close to the jet exit, the temperature measured from the schlieren technique differs from the thermocouple measurements, but with increasing downstream distance the agreement improves for the full radial profile of the temperature with the thermocouple measurements being within the error bars of the schlieren-derived temperature. We, also, note that the reconstructed temperature agrees well with the thermocouple measurements in identifying the level and the location of the peak temperature. Consequently, we can conclude that the developed approach for the processing of the schlieren measurements to derive the temperature of an ideal gas, using the methodology described earlier, is satisfactory. In the engine measurements that follow, however, the assumption of an axially symmetric temperature distribution cannot be invoked. Despite that, a qualitative assessment of the LOS-averaged temperature, with respect to the local temperature, can be made. We note that, in the hot air jet experiment, the maxima of the radial profiles of the LOS-averaged temperature and the local temperature coincide both in magnitude and radial location and we mention that the local temperature rises from ambient to higher values along a smooth boundary without steep gradients. In such a case, the maximum LOS-averaged temperature can provide a good estimate for the maximum local temperature along the line-of-sight and can, also, identify the spatial location of the highest local temperature in the direction normal to the light propagation. Both of these attributes are important for the interpretation of the engine measurements that follow.

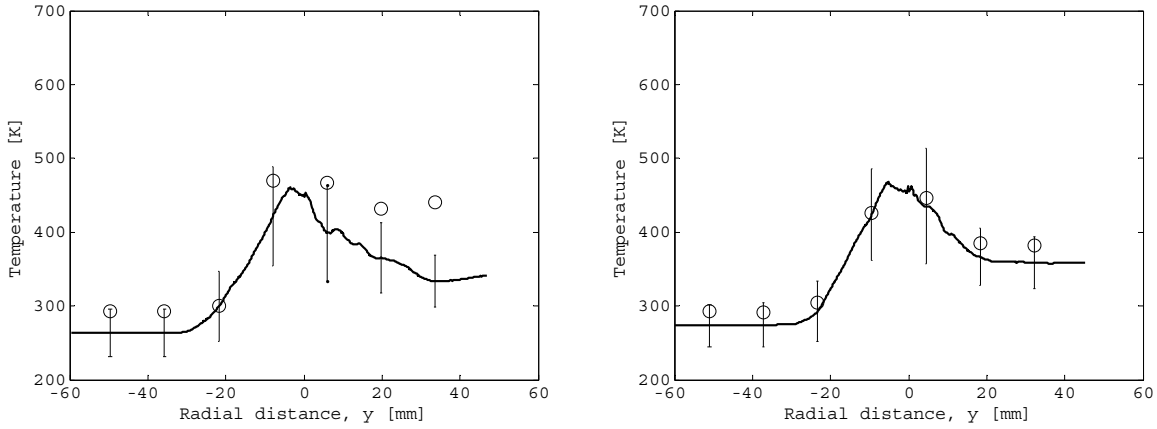

Fig. 13. Comparison between the thermocouple measurements (circles) and the schlieren-derived temperature (solid line), for the heated air jet experiment. The error bars correspond to the uncertainties calculated with the procedure outlined in the text. The distance downstream of the jet exit is 14mm (left) and 56mm (right).

6. Spark ignition engine experiments

A. LOS temperature distribution of the reaction zone

Using Equation 8, we showed in section 0 that LOS-averaged temperature variations of a hot air jet can be calculated. We then proceeded to test our method by measuring the temperature distribution of the reaction zone in a SI engine. An indication of the temperature of the burnt gases in a SI engine was obtained from calculations of the adiabatic flame temperature [25] using the NASA equilibrium program, [26, 27]. The adiabatic flame temperature for stoichiometric combustion of iso-octane for the current engine operating conditions was 2300K. Furthermore, [28] showed that the reaction zone can be identified within the schlieren image from the position of maximum deflection angle that varies depending on the shape of the reaction zone (*i.e.* concave or convex towards the hot gases). The position of the maximum deflection angle can be calculated by evaluating the integral [28]:

$$\varepsilon_y = -2y \int_y^{r_0} \frac{Ky}{\sqrt{r^2 - y^2}} dr \qquad \text{Equation 14}$$

where r is the radius of an axially symmetrical flame and K is the distribution of the refractive indices based on the pre-reaction zone temperature profile and equating it to zero. K was set as $\frac{(n_u-1)T_u S_u}{a}\left(\frac{T-T_u}{T^2}\right)$, where S is the burning velocity [29], α is the thermal diffusivity and subscript u denotes the cold, unburned state at 650K (assuming polytropic compression from Bottom Dead Centre (BDC) – 0.6bar and 295K at BDC). We calculated that the maximum deflection occurred at a temperature of 730 K for a convex reaction zone (i.e. the rays propagate through a "convex" boundary separating the unburnt region with the burnt gases in the centre of the combustion chamber) and at 1320 K for a concave reaction zone (i.e. the rays propagate through a "concave" boundary separating the unburnt region with the burnt gases in the centre of the combustion chamber). In an engine, however, the reaction zone is not generally, topologically simple. We therefore assumed that in a schlieren image, maximum deflection indicated the reaction zone position within the schlieren image and that the LOS temperature distribution of the reaction zone would lie between 730 and 1320 K.

B. Simulation of the effect of temperature, Air-to-Fuel ratio (A/F) and Exhaust Gas recirculation (EGR) variations on deflection angle

Unlike the case of the hot air gun experiment, where any variations in the schlieren image were only due to temperature distributions, in a combustion chamber, in addition to temperature variations, the presence of A/F

and EGR variations would also affect ε_y to some extent. Thus, before proceeding to the experimental work, the effect of temperature, A/F and EGR variations on ε_y was investigated computationally. This was also used to evaluate whether our assumption that the density gradients in the combustion chamber were primarily affected by temperature gradients was correct, and that the effect of A/F and EGR variations can be neglected. The refractive index of the different mixtures was calculated by considering the refractive indices [2] of both the reactants and the products in a SI engine based on the A/F and the EGR percentage [25].

In order to examine the effect of temperature, A/F and EGR variations on ε_y, the maximum deflection of a light beam passing through a 5mm diameter hot spot (the typical size of an expected inhomogeneity) in an engine was calculated. This was simulated by varying two of the three variables (A/F was varied from 10 to 20, EGR was varied from 0 to 10% and the temperature from 600 to 700K – since we operate the engine in this range of A/F and EGR and expect this range of pre-ignition temperatures) within the hot spot while keeping the third at a particular reference (i.e. A/F=15, EGR=0% and Temperature=650K), as shown in Fig. 14.

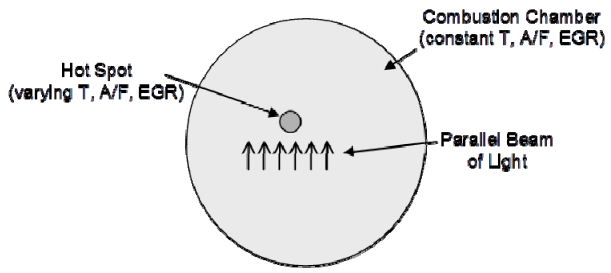

Fig. 14. Schematic of a hot spot of varying temperature, Air-to-Fuel ratio (A/F) and Exhaust Gas Recirculation (EGR) within an engine combustion chamber of constant temperature, A/F and EGR.

The results are shown in the 3 graphs of Fig. 15, which demonstrate that the temperature variations are the primary cause of refraction whereas EGR variations have minimal effect on the deflections. We calculated that, for our engine conditions (analysed later in this section), a 30% change in A/F caused the same deflections as a 4.5% change in temperature from the constant values and that a 100% change in EGR caused the same deflections as a 1.5% change in temperature. By considering the results from our sensitivity analysis, it can be argued that the deflection observed in the schlieren images was caused primarily by the temperature change, since typical variations of A/F and EGR in engines are much smaller than those considered above.

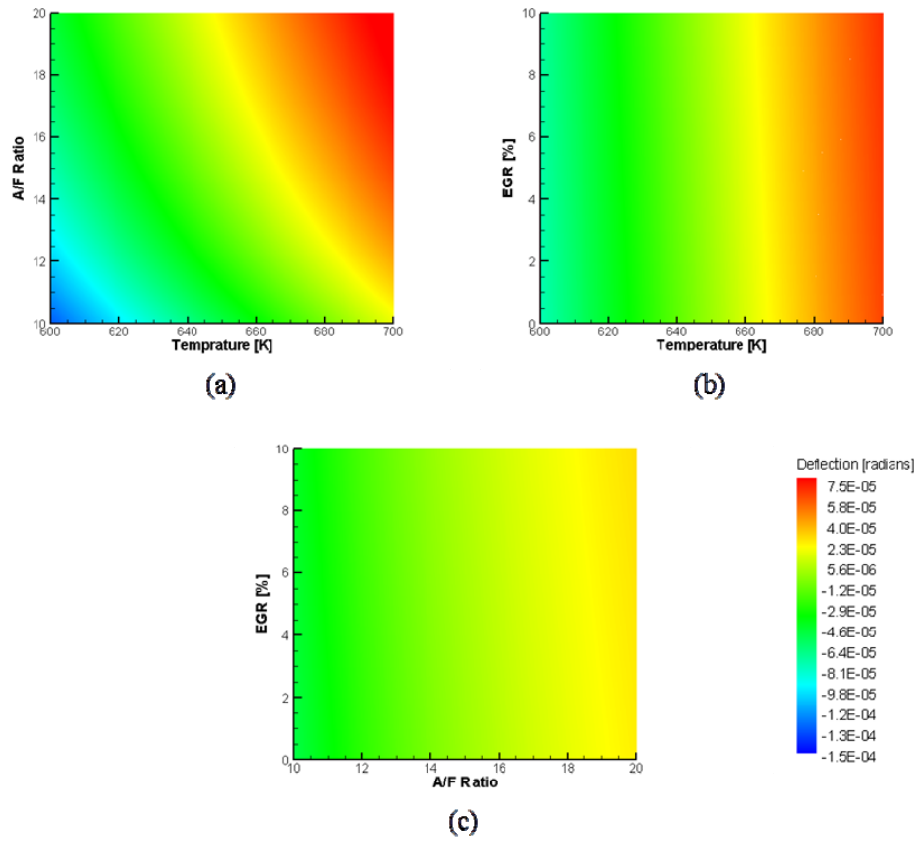

Fig. 15. Effect of (a) temperature, (b) A/F and (c) EGR on beam deflection, ε_y, during schlieren measurements.

C. Honda VTEC-E engine and optimised optical access

The experiments were conducted in a four-stroke, single-cylinder, optical SI engine with a four-valve, pentroof-type, Honda Variable valve Timing and lift Electronic Control (VTEC) cylinder head. The engine was designed by Honda R&D Co. Ltd., Japan (Engine No BKR-4). The engine had similar characteristics to a mass production SI with some minor differences. Those differences and the geometrical characteristics of the engine are summarised in Table 1. A more detailed description of the research engine can be found in [30].

Table 1 Engine Geometrical Characteristics.

CHARACTERISTIC PARAMETER	RESEARCH ENGINE (BKR-4)	PRODUCTION ENGINE
No of Cylinders	1 with Optical Access	4 in Line
Displacement Volume [cm^3]	360	1493
Compression Ratio	7.9	9.3
Bore × Stroke [mm × mm]	75 × 81.5	75 × 84.5
No of Valves/Cylinder	4 (2 Inlet, 2 Exhaust)	4 (2 Inlet, 2 Exhaust)

Valve Mechanism	SOHC VTEC-E	SOHC VTEC-E
Primary Inlet Valve Lift [mm]	8.00	8.00
Secondary Inlet Valve Lift [mm]	0.65	Min 0.65, Max 8.00
Exhaust Valve Lift [mm]	6.50	6.50

As was presented in Section 2, depending on the positioning of the knife edge (vertical or horizontal), rays are cut off in the direction vertical to the knife edge. Thus, the design of the optical window is very important, since any curvature (or imperfections) in the direction vertical to the knife edge would not allow for any measurements. In our case, the two curved windows providing optical access within the combustion chamber had no imperfections and no surface curvature vertical to the knife edge (i.e. parallel to the piston movement. Furthermore, to eliminate the possibility of the curved windows acting like lenses, and thus making sure the beam of light was parallel within the combustion chamber, the original curved windows were redesigned. As shown in Fig. 16, the original curved windows acted as diverging lenses, and no measurements could be obtained. However, by modifying the outer curvature of the windows (the inner curvature is dictated by the engine bore) we were able to get an almost parallel beam of light (a slight deviation of 1.5mm in over a 1.3m beam path).

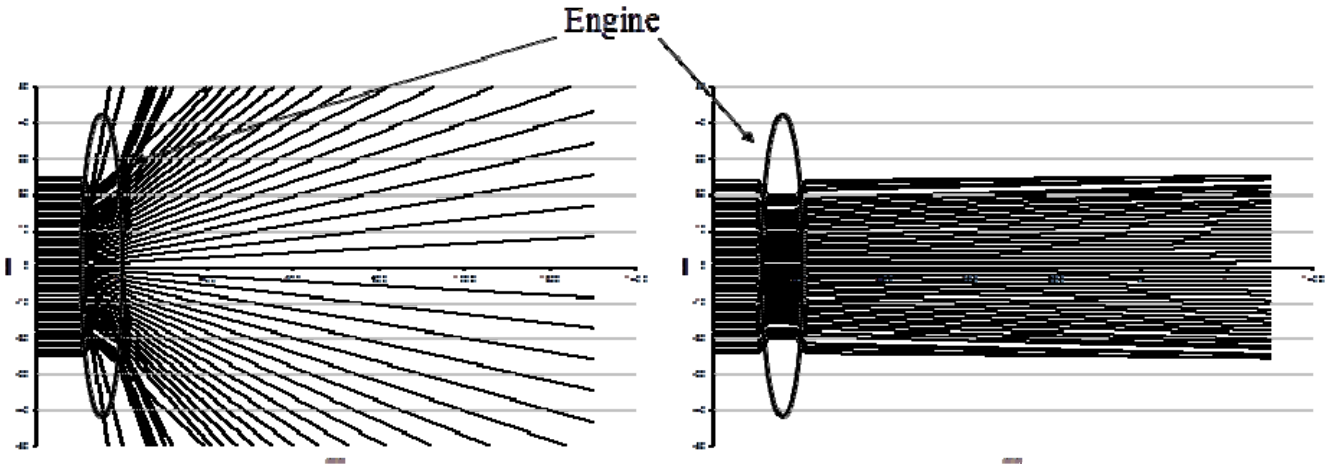

Fig. 16. Beam deviation through the combustion chamber before (left) and after (right) the redesigning of the curved quartz windows of the SI engine.

D. Optical setup

The experimental setup for the IC engine experiments consisted of simultaneous acquisition of natural light flame images and schlieren images. A schematic of the camera arrangements is illustrated in Fig. 17, where the Z-type schlieren system was set up to detect the flame inside the pentroof; a photograph of the combustion chamber through the pentroof windows and the piston is shown in Fig. 18. In Fig. 17, CCD camera 1 was used to record the chemiluminescent emissions of the flames through the pentroof window with the use of a half silvered mirror simultaneously with the acquisition of the schlieren images from CCD camera 2. The images were acquired using

CCD cameras coupled with a variable-gain image intensifier. The CCD cameras were coupled with a Nikon UV-Nikkor 105mm, f/4.5 lens for the flame images and a Nikon UV-Nikkor 35mm, f/4.5 lens for the schlieren images. The intensified system was able to detect the chemiluminescent emissions from the lean-burn, low-load engine operation flames, which emit weak intensities and are not easy to detect [31].

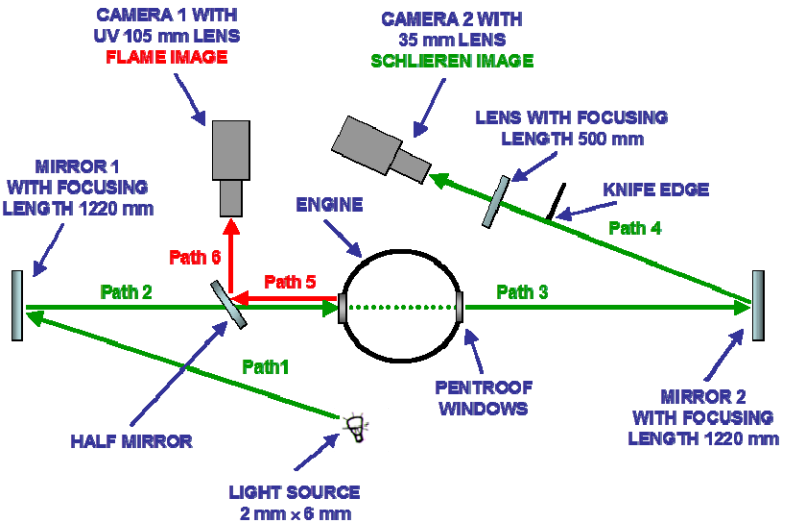

Fig. 17. Optical arrangement for simultaneous acquisition of schlieren and natural-light flame images in the cylinder of the spark ignition engine.

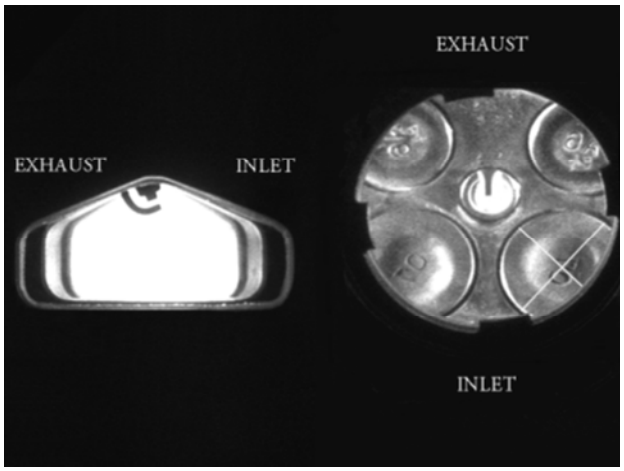

Fig. 18. The combustion chamber, as seen from the pentroof windows (left) and from the piston window (right). X denotes the primary inlet valve.

Mirrors with a different focal length than the hot air gun experiment (focal length: 1220mm instead of 3000mm) were used due to space limitations in our laboratory. Also, the angle between optical paths 1 and 2 and between

optical paths 3 and 4 was increased to 15º so that the beam path will not be obstructed by the engine block. Despite the shorter focal length the f-number of the mirrors is larger than 8, allowing the generation of good quality schlieren images. The larger tilting angles would produce increased astigmatism (coma, however, is not an issue when using the same tilting angles in a z-type configuration); we verified that astigmatism has been kept as low as possible, by checking that the darkening of the schlieren image is uniform as we translated the knife edge position [1]. A personal computer was used for the data acquisition and two PCs for the image acquisition that were synchronised by programming a timer board (Analogic CTRTM-10) to produce the appropriate triggering pulses after receiving the reference pulse from the engine.

Only one image per consecutive cycle could be acquired due to the 25 frames per second framing rate of the CCD camera. The image intensifiers were gated at a certain crank angle degree for 1°CA to record the natural light emitted by the flame. For an engine speed of 1500RPM this duration corresponded to 0.111ms. The images were digitised with 8-bit resolution into 256 grey scales with a size of 768×576 pixels.

E. Operating conditions

The injection timing used (40ºCA before Top Dead Centre (TDC)) was the same as suggested by [32, 33], in order to minimise cycle by cycle variations of the Indicated Mean Effective Pressure (IMEP) for lean burn SI operation. The engine was operated at 1500RPM with *iso*-octane fuel for consistency with previous experiments with the same engine in SI combustion mode [34]. The Volumetric Efficiency remained constant throughout the experiments at 30%.

7. Simultaneous in-cylinder flame and temperature measurements

Typical naturally emitted light images of the flame and the simultaneously acquired schlieren images are presented in Fig. 19. The images were acquired at 20° CA After Ignition Timing (i.e 20° CA before TDC) at A/F=15. The random nature of the development of the flames can be seen from both flame and schlieren images. The area of the “disturbed field” in the schlieren images is greater than the flame size in the natural images. This is due to the fact that hot gases ahead of the reaction zone caused changes in the density of the field and thus were identified by schlieren. Furthermore, there are no hot spots in the unburned mixture as indicated by the schlieren images, which is expected.

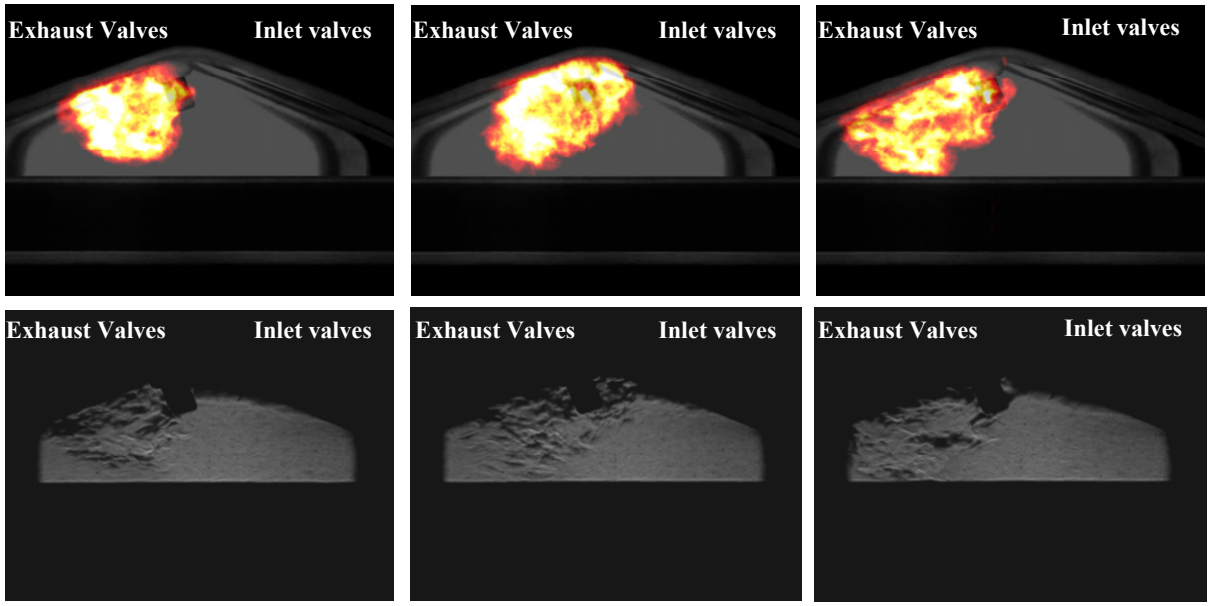

Fig. 19. Simultaneous flame and schlieren images at 20° CA after ignition timing for engine operation with A/F=15.

The LOS temperature distribution in the SI engine is presented in Fig. 20 and was measured from the schlieren images after processing according to the method previously described in Section 0. *L(x)* was equal to the length of the beam path through the engine at any given position in the x-direction. The datum line for the integration of Equation 8 was set at the lower visible part of the pentroof windows and the LOS temperature along the datum line was approximated to be 650K, assuming polytropic compression from BDC.

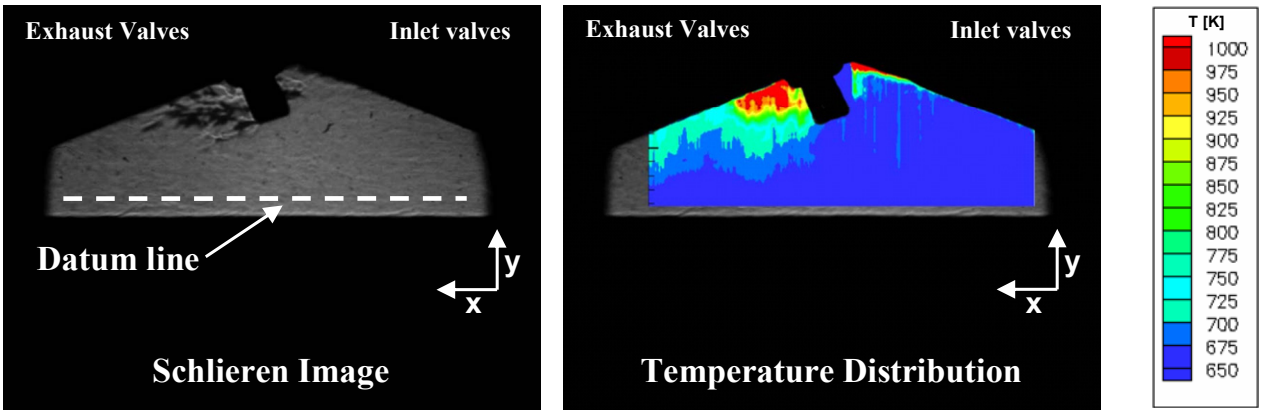

Fig. 20. Schlieren image and corresponding LOS temperature distribution at 20° CA after ignition for engine operation with A/F=15.

On the inlet-valve side of the spark plug, the temperature of the gases is almost constant. On the exhaust-valve side of the spark plug the LOS-averaged temperature profile of the flame can be measured. Hot gases were visible in front of the reaction zone at a temperature of about 700K and the maximum temperature of the burnt gases was over 1000K, however lower than the adiabatic flame temperature. Furthermore, at the position of maximum deflection (i.e. within the reaction zone) in the schlieren images, the temperature varied between 850 and 950K. This was in very good agreement with our calculations based on the maximum deflection theory [28], as presented in Section A. It was shown that the maximum deflection indicated the reaction zone position within the schlieren image and that the LOS temperature distribution of the reaction zone would be between 730 and 1320 K. Since the flame front is not of uniform shape and structure, one is unable to calculate the exact temperature of the flame front from the schlieren images. However, we believe that our processing of the schlieren images can be used to provide a very good approximation of the LOS gas temperature distribution in the cylinder of the SI engine.

8. Summary

The purpose of the paper is to demonstrate temperature measurements with schlieren in an internal combustion engine and evaluate the uncertainties. To do so, a Z-type, curved-mirror schlieren system was designed to measure, non-intrusively, whole-field LOS-averaged temperature distributions in a Spark Ignition (SI) engine. The following summarise the main findings:

1. A methodology was developed to enable the measurement of temperature variations from schlieren images. The methodology was based on previous work by [18, 19].
2. The errors in the temperature measurement due to the LOS-averaged refractive index and its inverse relationship to temperature were shown to be dominated by the systematic error introduced through Equation 9. The temperature, compared to an arithmetic average, is shown to be underestimated by a maximum of 8% with errors for typical engine operating conditions around ~4%.
3. The concept of using the schlieren technique to measure temperature was validated in a heated air flow. The schlieren measurements were reconstructed using an Abel inversion algorithm and the estimated radial profiles of temperature agreed well with point thermocouple measurements, depending on the flow position.
4. Simulations showed that the effects of EGR and A/F ratio on the schlieren images were minimal under engine conditions compared to the temperature effect. A 30% change in A/F caused the same deflections as a 4.5% change in temperature and a 100% change in EGR caused the same deflections as a 1.5% change

in temperature under engine conditions. Since variations of A/F up to 10% are expected, the effect on the schlieren images is negligible.

5. Further simulations showed that the maximum deflection in a schlieren image indicated the reaction zone position and that the LOS temperature distribution of the reaction zone would be between 730 and 1320 K [28].
6. Experiments were conducted in a SI engine to measure the temperature distribution of the reaction zone of an *iso*-octane mixture 20ºCA before TDC. The LOS-averaged temperature distribution was calculated successfully from the schlieren images. Good agreement between the LOS temperature distribution and the theoretically evaluated temperature was shown. In addition, good qualitative agreement between schlieren and chemiluminescence images of the flame was obtained.

Acknowledgements

Honda R&D Co. Ltd provided financial support for the research. Yannis Hardalupas, Nikos Soulopoulos and Alex Taylor would also like to acknowledge support from EPSRC grant GR/R54767/01.

References

1. S. G. Settles, *Schlieren and Shadowgraphy Techniques* (McGraw-Hill, 2001).
2. F. J. Weinberg, *Optics of flames* (Butterworths, London, 1963).
3. C. Alvarez-Herrera, D. Moreno-Hernández, B. Barrientos-García, and J. A. Guerrero-Viramontes, "Temperature measurement of air convection using a Schlieren system," Optics & Laser Technology **41**, 233-240 (2009).
4. X. Xiao, I. K. Puri, and A. K. Agrawal, "Temperature measurements in steady axisymmetric partially premixed flames by use of rainbow schlieren deflectometry," Applied Optics **41**, 1922-1928 (2002).
5. A. Schwarz, "Multi-tomographic flame analysis with a schlieren apparatus," Measurement Science and Technology **7**, 406-413 (1996).
6. P. S. Greenberg, R. B. Klimek, and D. R. Buchele, "Quantitative rainbow schlieren deflectometry," Applied Optics **34**, 3810-3822 (1995).
7. T. Fujikawa, T. Ozasa, and K. Kozuka, "Development of Transparent Cylinder Engines for Schlieren Observation," (SAE International, 1988).
8. M. Weinrotter, E. Wintner, K. Iskra, T. Neger, J. Olofsson, H. Seyfried, M. Aldén, M. Lackner, F. Winter, A. Vressner, A. Hultqvist, and B. Johansson, "Optical Diagnostics of Laser-Induced and Spark Plug-Assisted HCCI Combustion," (SAE International, 2005).
9. S. A. Kaiser, V. M. Salazar, and A. A. Hoops, "Schlieren measurements in the round cylinder of an optically accessible internal combustion engine," Applied Optics **52**, 3433-3443 (2013).
10. X. Qin, X. Xiao, I. K. Puri, and S. K. Aggarwal, "Effect of varying composition on temperature reconstructions obtained from refractive index measurements in flames," Combustion and Flame **128**, 121-132 (2002).
11. X. Xiao, C. W. Choi, and I. K. Puri, "Temperature measurements in steady two-dimensional partially premixed flames using laser interferometric holography," Combustion and Flame **120**, 318-332 (2000).
12. M. R. Davis, "Measurements in a subsonic turbulent jet using a quantitative schlieren technique," Journal of Fluid Mechanics **46**, 631-656 (1971).
13. W. L. Howes, "Rainbow schlieren and its applications," Applied Optics **23**, 2449-2460 (1984).

14. A. Agrawal, K., N. Butuk, K., S. Gollahalli, R., and D. Griffin, "Three-dimensional rainbow schlieren tomography of a temperature field in gas flows," Applied Optics **37**, 479-485 (1998).
15. D. A. Feikema, "Quantitative rainbow schlieren deflectometry as a temperature diagnostic for nonsooting spherical flames," Applied Optics **45**, 4826-4832 (2006).
16. A. Ibarreta, F. and C.-J. Sung, "Flame temperature and location measurements of sooting premixed Bunsen flames by rainbow schlieren deflectometry," Applied Optics **44**, 3565-3575 (2005).
17. A. Martínez-González, D. Moreno-Hernández, and J. A. Guerrero-Viramontes, "Measurement of temperature and velocity fields in a convective fluid flow in air using schlieren images," Applied Optics **52**, 5562-5569 (2013).
18. B. Lewis and G. von Elbe, *Combustion, flames and Explosion of Gases* (Academic Press, New York, 1961).
19. R. J. Goldstein, *Measurement techniques in heat transfer* (McGraw-Hill, London, 1976).
20. W. Merzkirch and Y. Egami, "Density-Based Techniques," in *Springer Handbook of Experimental Fluid Mechanics*, C. Tropea, A. Yarin, and J. Foss, eds. (Springer Berlin Heidelberg, 2007), pp. 473-486.
21. W. Merzkirch, *Flow Visualization,* 2nd ed. (Academic Press, 1987).
22. I. H. Sneddon, *The use of integral transforms* (McGraw-Hill, 1972).
23. A. K. Agrawal, B. W. Albers, and D. W. Griffin, "Abel inversion of deflectometric measurements in dynamic flows," Applied Optics **38**, 3394-3398 (1999).
24. C. J. Dasch, "One-dimensional tomography - A comparison of Abel, onion-peeling and filtered backprojection methods," Applied Optics **31**, 1146-1152 (1992).
25. J. B. Heywood, *Internal combustion engine fundamentals* (McGraw-Hill, 1988).
26. S. Gordon and B. J. McBride, "Computer program for calculation of complex chemical equilibrium compositions and applications I. Analysis," (1994).
27. R. A. Svehla and B. J. McBride, "Fortran IV computer program for calculation of thermodynamic and transport properties of complex chemical systems," (1973).
28. D. Dunn-Rankin and F. Weinberg, "Location of the schlieren image in premixed flames: Axially symmetrical refractive index fields," Combustion and Flame **113**, 303-311 (1998).
29. M. Metghalchi and J. C. Keck, "Burning velocities of mixtures of air with methanol, isooctane and indolene at high-pressure and temperature," Combustion and Flame **48**, 191-210 (1982).
30. P. G. Aleiferis, A. M. K. P. Taylor, J. H. Whitelaw, K. Ishii, and Y. Urata, "Cyclic variations of initial flame kernel growth in a Honda VTEC-E lean-burn spark-ignition engine," in *SAE 2000 World Congress,* (2000), pp. SAE 2000-2001-1207.
31. A. Nakamura, K. Ishii, and T. Sasaki, *Application of image converter camera to measure flame propagation in S. I. engine* (1989), Vol. 890322, p. Medium: X; Size: Pages: (10 p).
32. Y. Hardalupas, A. M. K. P. Taylor, J. H. Whitelaw, K. Ishii, H. Miyano, and Y. Urata, "Influence of injection timing on in-cylinder fuel distribution in a Honda VTEC-E engine," in *SAE International Congress and Exposition,* (1995).
33. N. E. Carabateas, "Two-phase flow and combustion is SI engines," (PhD, University of London, 1997).
34. P. G. Aleiferis, "Initial flame development and cyclic variations in a lean-burn spark-ignition engine," (PhD, University of London, 2000).